Asymmetric Warming/Cooling Response to CO_2 Increase/Decrease Mainly Due to Non-Logarithmic Forcing, not Feedbacks

Ivan Mitevski[1], Lorenzo M. Polvani[1,2], Clara Orbe[1,3]

[1]Department of Applied Physics and Applied Mathematics, Columbia University, New York, NY

[2]Lamont-Doherty Earth Observatory, Columbia University,Palisades, NY

[3]NASA Goddard Institute for Space Studies, New York, NY

Key Points:

- The global surface temperature responds asymmetrically to increased and decreased CO_2 levels, in both abrupt and transient cases
- Effective climate sensitivity is higher with warming ($2\times$, $4\times$, $8\times CO_2$) than with cooling ($1/2\times$, $1/4\times$, $1/8\times CO_2$), in two different coupled models
- The non-logarithmic nature of the CO_2 forcing is primarily responsible for the asymmetry, not the radiative feedbacks

Corresponding author: Ivan Mitevski, `im2527@columbia.edu`

Abstract

We explore the CO_2 dependence of effective climate sensitivity (S_G) with symmetric abrupt and transient CO_2 forcing, spanning the range $1/8\times$, $1/4\times$, $1/2\times$, $2\times$, $4\times$, and $8\times CO_2$, using two state-of-the-art fully coupled atmosphere-ocean-sea-ice-land models. In both models, under abrupt CO_2 forcing, we find an asymmetric response in surface temperature and S_G. The surface global warming at $8\times CO_2$ is more than one third larger than the corresponding cooling at $1/8\times CO_2$, and S_G is CO_2 dependent, increasing non-monotonically from $1/8\times CO_2$ to $8\times CO_2$. We find similar CO_2 dependence in the transient runs, forced with -1%$\mathrm{yr}^{-1}CO_2$ and +1%$\mathrm{yr}^{-1}CO_2$ up to $1/8\times CO_2$ and $8\times CO_2$, respectively. The non-logarithmic radiative forcing – not the changing feedbacks – primarily explains the dependence of S_G on CO_2, particularly at low CO_2 levels. The changing feedbacks, however, explain S_G's non-monotonic behavior.

Plain Language Summary

Equilibrium climate sensitivity (ECS) is the global mean warming after doubling CO_2 concentrations from those of the year 1850. Since CO_2 levels will likely surpass a doubling, it is crucial to know whether the amount of warming per CO_2 doubling (which we refer to as the effective climate sensitivity, S_G) is constant with each CO_2 doubling or whether it changes. Necessary conditions for constant S_G are 1) the radiative forcing introduced to the climate system from each CO_2 doubling is constant and 2) the net radiative feedback does not change with CO_2 levels. Current literature shows that S_G will increase in a warmer world because the radiative feedback will change. We here investigate S_G in both warmer and colder worlds, and confirm that S_G increases at higher CO_2 concentrations. However, we show that changes in the radiative forcing with each CO_2 doubling are mainly responsible for S_G increase with CO_2, not feedback changes.

1 Introduction

Equilibrium climate sensitivity (ECS) is the global mean surface temperature change after the doubling of CO_2 concentrations from pre-industrial (PI) levels. ECS is perhaps the most important metric in climate science, and it has been extensively investigated in the literature (Sherwood et al., 2020). An important question is whether the amount of warming for each CO_2 doubling (which we refer to as the effective climate sensitivity, S_{G}) is constant or not (i.e., whether it is CO_2 dependent). Necessary conditions for a constant S_{G} are 1) that the radiative forcing of the climate system for each CO_2 doubling is constant and 2) that the net radiative feedback does not change with CO_2 levels. This question has been investigated in many modeling studies (Meraner et al., 2013; Mauritsen et al., 2019; Sherwood et al., 2020; Bloch-Johnson et al., 2021), which have reported that S_{G} is indeed CO_2 dependent. Most of these studies find that S_{G} increases at higher CO_2 levels and that the change in feedbacks, not the change in CO_2 radiative forcing, is the primary driver of S_{G} CO_2 dependence.

An alternative approach to using climate models to investigate the dependency of S_{G} on CO_2 is to seek observational constraints from reconstructions of past climates. In particular, most studies conclude that S_{G} inferred from paleoclimate records does depend on CO_2 (Caballero & Huber, 2013; Anagnostou et al., 2016; Shaffer et al., 2016; Friedrich et al., 2016; Farnsworth et al., 2019; Zhu et al., 2019; Anagnostou et al., 2020), although a few studies disagree (e.g., Martínez-Botí et al. (2015)). An ideal period to study the S_{G} from past climate is the Last Glacial Maximum (LGM), approximately 21 kyr ago, when the Earth was roughly 6K colder than PI conditions (Tierney et al., 2020). The LGM period is of particular interest because the climate system was in a quasi-equilibrium state, the climate forcings were large, and the surface temperature reconstructions are relatively well-constrained (Zhu & Poulsen, 2021). However, when considering the LGM and other periods in Earth's past, one needs to account for how the feedbacks in those past climate states differ from the feedbacks operating in the modern state: hence the challenge in using paleoclimate-based estimates to constrain S_G.

While modeling and paleoclimatic evidence suggest that S_G depends on CO_2, a systematic exploration of the symmetry over a wide range of CO_2 forcing has yet to be performed. The question thus remains: is the climate system response symmetric across a broad range of positive (warm) and negative (cold) CO_2 forcings? The question of symmetry was examined recently by Chalmers et al. (2022), who compared $1/2\times$ and $2\times CO_2$ simulations performed with the CESM1-CAM5 model, and found that global surface temperatures warm 20% more than they cool. Roughly 50% of this asymmetry was shown to derive from an asymmetry in CO_2 radiative forcing; the rest was associated with differences in feedbacks which, interestingly, were found not to be related to clouds. Whether this result holds over a broader range of CO_2 forcing, and whether it is model dependent remains an open question.

We here address these questions using a much broader range of both abrupt and transient CO_2 forcings, and do so with two different climate models. Specifically, CO_2 is varied from $1/8\times$ to $8\times$PI values, to test the CO_2 symmetry of the climate system response to comparable increased and decreased CO_2. While we are not the first ones to perform such symmetric CO_2 runs (Hansen et al., 2005; Colman & McAvaney, 2009; Russell et al., 2013; Chalmers et al., 2022), here we explore 1) a larger CO_2 range than previously considered, 2) we do so using two different fully coupled climate models and, most importantly, 3) we perform the experiments with both abrupt and transient CO_2 runs.

Overall we confirm the asymmetric response in surface temperature: the climate system warms *more* with consecutive CO_2 doublings ($2\times$, $4\times$, and $8\times CO_2$) than it cools with consecutive CO_2 halvings ($1/2\times$, $1/4\times$, and $1/8\times CO_2$). This asymmetry is also reflected in S_G, which *increases* at higher CO_2 concentrations, consistent with previous studies. Surprisingly, we find that the non-logarithmic dependence of CO_2 radiative forcing (i.e., the fact that CO_2 radiative forcing increases more rapidly than the log of the CO_2 concentration) is primarily responsible for this asymmetric response, and not the changes in radiative feedbacks.

2 Methods

2.1 Models Used

We use two fully coupled atmosphere-ocean-sea-ice-land models: the large ensemble version of the Community Earth System Model (CESM-LE) and the NASA Goddard Institute for Space Studies Model E2.1-G (GISS-E2.1-G). CESM-LE comprises the Community Atmosphere Model version 5 (CAM5, 30 vertical levels), and parallel ocean program version 2 (POP2, 60 vertical levels) with approximately 1° horizontal resolution in all model components (Kay et al., 2015). GISS-E2.1-G is a 40-level atmospheric model with a resolution of 2° × 2.5° latitude/longitude, coupled to a 1° horizontal resolution 40-level GISS Ocean v1 (GO1) (Kelley et al., 2020). This configuration of the GISS model contributed to the CMIP6 project under the label "GISS-E2-1-G". We show CESM-LE results in the main text, and some GISS-E2.1-G results in supplementary information (SI) to corroborate CESM-LE findings.

2.2 Abrupt $n\times CO_2$ Experiments

We perform a series of abrupt CO_2 forcing runs using both models, subject to $1/8\times$, $1/4\times$, $1/2\times$, $2\times$, $4\times$, and $8\times CO_2$ forcings, with all other trace gases, ozone concentrations, aerosols, and other forcings fixed at PI values. Following CMIP6 protocol for $4\times CO_2$ runs, we integrate all runs to 150 years starting from PI conditions. We contrast these to a PI control run to calculate the response.

For each model, we estimate the effective radiative forcing (ERF) with a companion series of CO_2 experiments, as per Forster et al. (2016), with prescribed PI sea surface temperatures (SSTs) and sea-ice concentrations (SICs). These experiments are 30-year-long. We calculate ERF as the difference between the global mean net top of the atmosphere (TOA) flux between PI and $n\times CO_2$ in these prescribed SSTs and SICs experiments. We do not here adjust for land warming simply because, in our ERF calculations, the surface temperature response in the fixed SSTs and SICs simulations is minimal (Smith et al., 2020), but we have verified that the adjustment does not change our results (see Figure S3).

2.3 Transient Experiments

In addition to the abrupt CO_2 runs, we also perform transient CO_2 runs with the CESM-LE model. We start from PI conditions (same as in the abrupt CO_2 forcing), and we increase CO_2 at $+1\%\text{yr}^{-1}$ for the "warm" case for 215 years (slightly above $8{\times}CO_2$) and $-1\%\text{yr}^{-1}$ for the "cold" case for 215 years (slightly below $1/8{\times}CO_2$). We estimate transient effective radiative forcing as in the abrupt experiments, by running companion simulations with specified SSTs and SICs set to PI values (Forster et al., 2016), while ramping up CO_2 at rates of $+1\%\text{yr}^{-1}$ and $-1\%\text{yr}^{-1}$. We contrast all variables to PI values to compute the response.

2.4 Climate Sensitivity & Feedbacks

We define effective climate sensitivity S_G as the x-intercept of the Gregory regression (Gregory et al., 2004) for each abrupt $n \times CO_2$ run using the following equation:

$$S_\text{G} = \left| \frac{F_{\text{y}-\text{int}}(n \times \text{CO}_2)}{\lambda(n \times \text{CO}_2) \cdot \log_2 n} \right| \tag{1}$$

We find the radiative forcing $F_{\text{y}-\text{int}}$ as the y-intercept and the net feedback parameter λ as the slope from the Gregory regression (see Figure S1) where we regress the net TOA radiative imbalance against the global mean surface temperature response for years 1-150. In order to compare S_G for different CO_2 doubling / halving, we divide by $\log_2 n$ (assuming a logarithmic CO_2 forcing) and take the absolute value in Equation 1. Note that our definition of the effective climate sensitivity S_G is a generalization of the more common definition of effective climate sensitivity (which is typically defined as per Equation 1 but with $n = 2$). To check for the posibility that λ and S_G may be strongly affected by the "pattern effect", we have repeated the calculations by regressing years 21-150 only, and our main results were not changed.

To calculate the individual feedbacks λ_i, we use radiative kernels (K_x) from both Pendergrass et al. (2018) and Huang et al. (2017) to quantify the sensitivity of TOA radiation imbalance (ΔR) to changes in surface and atmospheric temperature (T), water vapor (q), and surface albedo (α) (Soden et al., 2008; Shell et al., 2008). For each year of the 150-year experiment, we multiply the spatially-resolved kernels by the climate field anomalies ($R_x = K_x \cdot \Delta x$, where x is T, q, α), and then vertically integrate (for atmospheric temperature and water vapor) up to the tropopause. We define the tropopause as 100 hPa at the equator, 300 hPa at the poles, and in between, it varies by the cosine of the latitude (Soden & Held, 2006). Lastly, we regress these quantities on the surface temperature response to find the radiative feedbacks as the regression slope. The cloud feedbacks are computed via the residual method (Soden & Held, 2006) as follows. First, we subtract effective radiative forcing and the temperature, water vapor, and surface albedo radiative fluxes from the TOA net radiative flux, resulting in $\Delta R_{\text{cloud}} = \Delta R - \text{ERF} - \sum \Delta R_x$. Then, we regress ΔR_{cloud} onto ΔT_s anomalies and define the corresponding slope as the cloud feedback. Lastly, we find shortwave (SW) and longwave (LW) components of the cloud feedback by considering the radiative changes in LW and SW components separately.

In the transient runs, we estimate the net feedback parameter λ_{tr} following Rugenstein and Armour (2021) (see λ_{eff1pct} in their Figure 1d) with the expression:

$$\lambda_{\text{tr}} = -\frac{\text{ERF}(t) - \Delta R(t)}{\Delta T_s(t)} \tag{2}$$

$\Delta R(t)$ is the net TOA radiative imbalance, and $\Delta T_s(t)$ is the global mean surface temperature response in the transient runs at year t. $\Delta R(t)$ and $\Delta T_s(t)$ are 30-year moving averages of the respective terms. Note that we use different definitions for the feedback parameter in the abrupt and transient simulations.

3 Results

3.1 Abrupt CO_2 Experiments

We start by examining the global mean surface temperature response ($|\Delta T_s|$) timeseries for the abrupt CO_2 runs (Figure 1). We contrast – in panels a, b, and c – the timeseries of each corresponding "warm" (2×, 4×, and 8×CO_2) and "cold" simulation (1/2×, 1/4×, and 1/8×CO_2) by taking the absolute value of the response from PI: note that the $|\Delta T_s|$ in the "warm" case is always stronger than the "cold" case. In particular, we find 20% more warming at 2× than cooling at 1/2×CO_2 (Figure 1a), 15% more at 4× than 1/4×CO_2 (Figure 1b), and 41% more at 8× than 1/8×CO_2 (Figure 1c). The asymmetry in $|\Delta T_s|$ is amplified at higher CO_2 forcing, and largest in the 1/8×CO_2 vs. 8×CO_2 case (Figure 1c). The asymmetry is reduced at 4×CO_2 vs. 1/4×CO_2 due to changes in ocean heat transport which result in a formation of the North Atlantic Warming Hole in this model at 4×CO_2 (see more details in Mitevski et al. (2021)).

To quantify the timescale of the asymmetry in $|\Delta T_s|$ between "warm" and "cold" cases, we define the asymmetry between "warm" and "cold" cases as

$$\Delta_a X = |\Delta X(\text{warm})| - |\Delta X(\text{cold})| \tag{3}$$

where X is any climate variable (e.g., T_s), and subscript a refers to "asymmetry" (Figure 1d). In particular, we find that the asymmetry emerges rapidly in the first ten years (e.g., 90% at 8×CO_2). Relative to the (slower) response associated with SST-driven feedbacks, the asymmetry appears quickly, suggesting that it might be due to radiative changes.

Next, we calculate effective climate sensitivity S_G from the Gregory regression (Equation 1), and plot it as percentage change from 2×CO_2 (black line, Figure 2a). S_G is CO_2 dependent and increases with CO_2 concentration: at 1/8×CO_2, it is more than 20% *lower* than 2×CO_2 values, and at 8×CO_2, it is around 5% *higher* than at 2×CO_2. CO_2 dependent S_G is possible if either the effective radiative forcing (ERF) or the net feedback parameter (λ) change with CO_2. To individually test the relative importance of ERF and λ, we calculate the climate sensitivity in two different ways.

First, to examine the dependence of climate sensitivity on ERF, we calculate climate sensitivity as S_F using the expression:

$$S_F = \left| \frac{\text{ERF}(n \times CO_2)}{\lambda(2 \times CO_2) \cdot \log_2 n} \right| \tag{4}$$

where ERF is derived from the $n \times CO_2$ fixed SSTs and SICs runs, and λ (slope from Gregory Regression) is held constant at the $2{\times}CO_2$ value. As seen in Figure 2a, we find that S_F (blue line) changes in tandem with S_G (black line), which reinforces the fact that changes in ERF explain the changes in S_G.

Second, to assess whether changes in feedback strength also contribute to S_G, we calculate climate sensitivity as S_λ:

$$S_\lambda = \left| \frac{\text{ERF}(2 \times CO_2)}{\lambda(n \times CO_2)} \right| \tag{5}$$

where λ is calculated at each $n \times CO_2$ and ERF is held constant at $2{\times}CO_2$ value. As seen in Figure 2a, S_λ (red) changes in the opposite direction than S_G (black) for CO_2 values lower than $2{\times}CO_2$. This suggests that changes in λ are not the main driver of the S_G dependence on CO_2. However, it is important to note that for CO_2 values higher than $2{\times}CO_2$, we find λ non-monotonically increasing to $8{\times}CO_2$, which can be linked to the corresponding non-monotonic behavior of S_G. We find qualitatively similar results using the GISS-E2.1-G model (Figure S2a), confirming that ERF is the primary driver of the dependence of S_G on CO_2.

Next, we correlate S_G with $1/\lambda$ (Figure 2c) and ERF (Figure 2d) across all abrupt CO_2 experiments from $1/8\times$ to $8{\times}CO_2$ to examine whether feedbacks or forcing better correlate with changes in S_G. Overall, we find little correlation between S_G and $1/\lambda$ (r=-0.44) and a very strong correlation between S_G and ERF (r=0.91). Similarly, a high correlation between S_G and ERF is found in the GISS-E2.1-G model (Figure S2d). This strengthens our conclusions from Figure 2a that the changes in ERF are driving the S_G increase. However, if one considers warm cases, one sees a strong correlation between S_{G} and $1/\lambda$, as indicated earlier. This is in agreement with previous studies (Meraner et al., 2013; Bloch-Johnson et al., 2021), which reported that feedback changes are important for the dependence of S_{G} on CO_2. However, over a broad range of CO_2 forcing, including colder climates, that is not the case: changes in ERF are more important than feedback changes.

Given the aforementioned importance of ERF in driving the changes in S_{G}, we next look in more detail at ERF, calculated from fixed SSTs and SICs runs, following Forster et al. (2016), from $^1/_8\times$ to $8\times CO_2$ (dark blue bars, Figure 2b). If ERF were scaled simply with the logarithm of CO_2 concentration, then the dark blue bars would be identical for all CO_2 values. However, we see that ERF grows more than logarithmically with CO_2. We find a similar but weaker non-logarithmic behavior in the instantaneous radiative forcing (IRF) reported in Byrne and Goldblatt (2014), which we obtain by linearly interpolating their line-by-line radiative calculations (SI file "text03.txt" in Byrne and Goldblatt (2014)) and plot with light blue bars in Figure 2b. We also compare our ERF calculations with the proposed stratospherically adjusted radiative forcing fit in Etminan et al. (2016) for the warming case only (since it is not valid for low CO_2 values), and it appears both are in agreement.

A limitation to our ERF calculation approach is that we only fix the SSTs and SICs in the simulation, but not the land temperatures. Fixing the land temperatures has been shown to increase ERF in warmer climates even more than when only SSTs and SICs are fixed (Andrews et al., 2021). To account for this, we removed the land and sea-ice warming effects in our ERF calculations, following Equation 1 in Hansen et al. (2005) as shown in Figure S3, and found that the correction (dashed blue lines) leads, if anything, to a stronger non-logarithmic ERF. Hence, incorporating fixed land temperatures leads to ERF increasing even more rapidly than the log of CO_2 concentration; this strengthens our argument that the S_{G} dependence on CO_2 is due to non-logarithmic CO_2 radiative forcing.

Next, we perform a standard decomposition of λ into individual radiative feedbacks λ_i. The summation of individual feedbacks ($\sum \lambda_i$) is shown in Figure 3a (blue). $\sum \lambda_i$ follows closely the net feedback calculated from the Gregory regression (black). We perform the decomposition using two radiative kernels from Pendergrass et al. (2018) and Huang et al. (2017), and we find minimal sensitivity to the choice of kernel (Figure S4). The individual feedbacks, plotted as differences from $2\times CO_2$ values, from the Pendergrass et al. (2018) kernels are shown in Figure 3b. We see a clear signal in the lapse rate feedback, which weakens the net feedback in the "cold" case and strengthens it in the "warm" case. The longwave cloud feedback has clear global surface temperature dependence, increasing with CO_2 monotonically for all CO_2 values. However, in general, we find no clear pattern in the changes in individual feedbacks that would sufficiently explain the overall feedbacks CO_2 dependence. In addition, the changes in feedbacks in the GISS-E2.1-G model (Figure S5) are qualitatively different from those in the CESM-LE model (Figure 3). Since our models do not agree on the changes in individual feedbacks across the CO_2 range, and since we showed that feedback changes are strongly not correlated with changes in S_G (Figure 2c), we do not explore further the mechanisms driving feedback changes in the individual models.

3.2 Transient CO_2 runs

The abrupt CO_2 forcing runs show that the effective climate sensitivity increases with CO_2, and that the non-logarithmic nature of the ERF is largely responsible for this behavior. Now we seek to determine whether the same behavior is also seen in runs with transient CO_2 forcing, which are much more realistic. Our transient runs are forced, starting from PI, with CO_2 concentrations increasing at the rate of $1\%\mathrm{yr}^{-1}$ and decreasing at $1\%\mathrm{yr}^{-1}$. As seen in Figure 4a, the surface temperature response $|\Delta T_s|$ is stronger in the warming (red) than in the cooling (blue) case. Note that the responses computed from the last 50 years of the abrupt simulations at the corresponding CO_2 value (dots) are a good predictor of the response in the transient runs, demonstrating that the results of the abrupt runs carry over to the transient runs. Together with the surface temperature, ERF also changes more rapidly in the warming than the cooling experiments, as seen in Figure 4b.

Next, we explore how the transient feedbacks (λ_{tr}, see Equation 2) change in the "warm" and "cold" cases (Figure 4c). The feedbacks timeseries are noisy at the beginning of the simulation, but in the last thirty years, the warm case shows 10% weaker (more positive) feedbacks compared to the cold case. The 10% difference indicates that S_{G} in the warming case should be higher than in the colder case. However, a robust difference in feedbacks only appears around year 130, whereas the $|\Delta T_s|$ asymmetry emerges much earlier, around year 60. This difference in the temporal evolution of the feedbacks, relative to the evolution of the forcing and S_{G}, adds additional strong evidence that the feedbacks are not driving the $|\Delta T_s|$ asymmetry.

Finally, as for the abrupt CO_2 runs, we correlate the asymmetry in global mean surface temperature response $\Delta_a T_s$ and effective radiative forcing Δ_aERF (Figure 4d). We find a correlation of r=0.96, suggesting that the asymmetric changes in ERF drive the $|\Delta T_s|$ asymmetry between the "cold" and "warm" cases. As we can see in Figure 4c, the transient feedbacks are contributing to the $|\Delta T_s|$ asymmetry at the end of the run, but their impact is much smaller than the one from ERF.

4 Summary and Discussion

We have explored the effective climate sensitivity (S_{G}) dependence on CO_2 with abrupt *and* transient CO_2 experiments spanning the range $1/8\times$ to $8\times CO_2$ using two distinct CMIP-class climate models. First, we have found a considerable asymmetry in surface temperature response, with the climate system warming more than cooling for identical factors used to increase and decrease the CO_2 concentration, starting from a pre-industrial climate. Second, we showed that the asymmetry is due to the non-logarithmic nature of CO_2 radiative forcing, not the feedback changes. Upon decomposing the total feedback into individual feedbacks, we found no simple explanation relating specific feedback changes to the changes in S_G across the $^1/_8\times$ to $8\times CO_2$ forcing range examined in this study.

Most studies to date have focused on the role of feedbacks in explaining the dependency of S_G on CO_2, with relatively little attention placed on radiative forcing. Indeed, consistent with these studies, we found that for warmer climates ($> 2 \times CO_2$), feedbacks are important for determining the changing behavior of S_G with CO_2. However, by considering a broader range of CO_2 forcings, we have shown here that for cases in which CO_2 concentrations are less than PI values, non-logarithmic ERF is the primary driver of S_G changes. Our goal here has been to isolate the role of CO_2 alone, and we have set all other forcings to PI values. Needless to say, we have ignored the "slow" feedbacks present in cold climates (e.g., the LGM), such as the formation of land ice sheets.

The results with our abrupt runs have been shown to be robust with two climate models for simulations up to 150 years. One may argue that our runs are not equilibrated, and we agree with that caveat. However, we have found that the asymmetry and the key role of ERF are also robustly seen in the transient runs. Because of this, we expect that prolonging the abrupt simulation for more than 150 years will yield similar results. In any case, it will be important to repeat similar experiments with longer simulations as in LongRunMIP (Rugenstein et al., 2019) to confirm that this asymmetry is still present at long times closer to equilibration. Finally, our findings indicate that future studies should place more emphasis on accurately quantifying the changes in effective radiative forcing when studying the effective climate sensitivity dependency on CO_2. The feedbacks appear unable to explain the cooling phase.

5 Open Research

The CESM-LE model data can be obtained at `https://doi.org/10.5281/zenodo.5725084` and GISS-E2.1-G model data at `https://doi.org/10.5281/zenodo.3901624`.

Acknowledgments

We thank Jennifer Kay (University of Colorado Boulder) for helping with the feedback calculations, Ian Eisenman (UC San Diego) and Kyle Armour (University of Washington) for suggesting the radiative forcing fit from Byrne and Goldblatt (2014), and two anonymous reviewers for constructive comments that improved the paper. This work was supported by NASA FINESST Grant 80NSSC20K1657. The work of LMP is supported, in part, by a grant from the US National Science Foundation to Columbia University. We thank the high-performance computing resources provided by NASA's Advanced Supercomputing (NAS) Division and the NASA Center for Climate Simulation (NCCS). Part of the computing and data storage resources, including the Cheyenne supercomputer (doi:10.5065/D6RX99HX), were provided by the Computational and Information Systems Laboratory at National Center for Atmospheric Research (NCAR).

References

Anagnostou, E., John, E. H., Babila, T. L., Sexton, P. F., Ridgwell, A., Lunt, D. J., … Foster, G. L. (2020, Sep 07). Proxy evidence for state-dependence of climate sensitivity in the eocene greenhouse. *Nature Communications*, *11*(1), 4436. doi: https://doi.org/10.1038/s41467-020-17887-x

Anagnostou, E., John, E. H., Edgar, K. M., Foster, G. L., Ridgwell, A., Inglis, G. N., … Pearson, P. N. (2016, May 01). Changing atmospheric co2 concentration was the primary driver of early cenozoic climate. *Nature*, *533*(7603), 380-384. doi: https://doi.org/10.1038/nature17423

Andrews, T., Smith, C. J., Myhre, G., Forster, P. M., Chadwick, R., & Ackerley, D. (2021). Effective radiative forcing in a gcm with fixed surface temperatures. *Journal of Geophysical Research: Atmospheres*, *126*(4), e2020JD033880. doi: https://doi.org/10.1029/2020JD033880

Bloch-Johnson, J., Rugenstein, M., Stolpe, M. B., Rohrschneider, T., Zheng, Y., & Gregory, J. M. (2021). Climate sensitivity increases under higher co2 levels due to feedback temperature dependence. *Geophysical Research Letters*, *48*(4), e2020GL089074. doi: https://doi.org/10.1029/2020GL089074

Byrne, B., & Goldblatt, C. (2014). Radiative forcing at high concentrations of well-mixed greenhouse gases. *Geophysical Research Letters*, *41*(1), 152-160. doi: https://doi.org/10.1002/2013GL058456

Caballero, R., & Huber, M. (2013). State-dependent climate sensitivity in past warm climates and its implications for future climate projections. *Proceedings of the National Academy of Sciences*, *110*(35), 14162–14167. doi: https://doi.org/10.1073/pnas.1303365110

Chalmers, J., Kay, J. E., Middlemas, E., Maroon, E., & DiNezio, P. (2022). Does disabling cloud radiative feedbacks change spatial patterns of surface greenhouse warming and cooling? *Journal of Climate*. doi: https://doi.org/10.1175/JCLI-D-21-0391.1

Colman, R., & McAvaney, B. (2009). Climate feedbacks under a very broad range of forcing. *Geophysical Research Letters*, *36*(1). doi: https://doi.org/10.1029/2008GL036268

Etminan, M., Myhre, G., Highwood, E. J., & Shine, K. P. (2016). Radiative forcing of carbon dioxide, methane, and nitrous oxide: A significant revision of the methane radiative forcing. *Geophysical Research Letters*, *43*(24), 12,614-12,623. doi: https://doi.org/10.1002/2016GL071930

Farnsworth, A., Lunt, D. J., O'Brien, C. L., Foster, G. L., Inglis, G. N., Markwick, P., ... Robinson, S. A. (2019). Climate sensitivity on geological timescales controlled by nonlinear feedbacks and ocean circulation. *Geophysical Research Letters*, *46*(16), 9880-9889. doi: https://doi.org/10.1029/2019GL083574

Forster, P., Richardson, T., Maycock, A. C., Smith, C. J., Samset, B. H., Myhre, G., ... Schulz, M. (2016). Recommendations for diagnosing effective radiative forcing from climate models for cmip6. *Journal of Geophysical Research: Atmospheres*, *121*(20), 12,460-12,475. doi: https://doi.org/10.1002/2016JD025320

Friedrich, T., Timmermann, A., Tigchelaar, M., Elison Timm, O., & Ganopolski, A. (2016). Nonlinear climate sensitivity and its implications for future greenhouse warming. *Sci-*

ence Advances, *2*(11). doi: https://doi.org/10.1126/sciadv.1501923

Gregory, J. M., Ingram, W. J., Palmer, M. A., Jones, G. S., Stott, P. A., Thorpe, R. B., … Williams, K. D. (2004). A new method for diagnosing radiative forcing and climate sensitivity. *Geophysical Research Letters*, *31*(3). doi: https://doi.org/10.1029/2003GL018747

Hansen, J., Sato, M., Ruedy, R., Nazarenko, L., Lacis, A., Schmidt, G. A., … Zhang, S. (2005). Efficacy of climate forcings. *Journal of Geophysical Research: Atmospheres*, *110*(D18). doi: https://doi.org/10.1029/2005JD005776

Huang, Y., Xia, Y., & Tan, X. (2017). On the pattern of co2 radiative forcing and poleward energy transport. *Journal of Geophysical Research: Atmospheres*, *122*(20), 10,578-10,593. doi: https://doi.org/10.1002/2017JD027221

Kay, J. E., Deser, C., Phillips, A., Mai, A., Hannay, C., Strand, G., … Vertenstein, M. (2015, 09). The Community Earth System Model (CESM) Large Ensemble Project: A Community Resource for Studying Climate Change in the Presence of Internal Climate Variability. *Bulletin of the American Meteorological Society*, *96*(8), 1333-1349. doi: https://doi.org/10.1175/BAMS-D-13-00255.1

Kelley, M., Schmidt, G. A., Nazarenko, L. S., Bauer, S. E., Ruedy, R., Russell, G. L., … Yao, M.-S. (2020). Giss-e2.1: Configurations and climatology. *Journal of Advances in Modeling Earth Systems*, *12*(8), e2019MS002025. doi: https://doi.org/10.1029/2019MS002025

Martínez-Botí, M. A., Foster, G. L., Chalk, T. B., Rohling, E. J., Sexton, P. F., Lunt, D. J., … Schmidt, D. N. (2015). Plio-pleistocene climate sensitivity evaluated using high-resolution CO2 records. *Nature*, *518*(7537), 49-54. doi: https://doi.org/10.1038/nature14145

Mauritsen, T., Bader, J., Becker, T., Behrens, J., Bittner, M., Brokopf, R., … Roeckner, E. (2019). Developments in the mpi-m earth system model version 1.2 (mpi-esm1.2) and its response to increasing co2. *Journal of Advances in Modeling Earth Systems*, *11*(4), 998-1038. doi: https://doi.org/10.1029/2018MS001400

Meraner, K., Mauritsen, T., & Voigt, A. (2013). robust increase in equilibrium climate sensitivity under global warming. *geophysical research letters*, *40*(22), 5944-5948. doi: https://doi.org/10.1002/2013gl058118

Mitevski, I., Orbe, C., Chemke, R., Nazarenko, L., & Polvani, L. M. (2021). Non-monotonic response of the climate system to abrupt co2 forcing. *Geophysical Research Letters*, *48*(6), e2020GL090861. doi: https://doi.org/10.1029/2020GL090861

Pendergrass, A. G., Conley, A., & Vitt, F. M. (2018). Surface and top-of-atmosphere radiative feedback kernels for cesm-cam5. *Earth System Science Data*, *10*(1), 317–324. doi: https://doi.org/10.5194/essd-10-317-2018

Rugenstein, M., & Armour, K. C. (2021). Three flavors of radiative feedbacks and their implications for estimating equilibrium climate sensitivity. *Geophysical Research Letters*, *48*(15), e2021GL092983. doi: https://doi.org/10.1029/2021GL092983

Rugenstein, M., Bloch-Johnson, J., Abe-Ouchi, A., Andrews, T., Beyerle, U., Cao, L., … Yang, S. (2019). Longrunmip: Motivation and design for a large collection of millennial-length aogcm simulations. *Bulletin of the American Meteorological Society*, *100*(12), 2551 - 2570. doi: https://doi.org/10.1175/BAMS-D-19-0068.1

Russell, G. L., Lacis, A. A., Rind, D. H., Colose, C., & Opstbaum, R. F. (2013). Fast atmosphere-ocean model runs with large changes in co2. *Geophysical Research Letters*, *40*(21), 5787-5792. doi: https://doi.org/10.1002/2013GL056755

Shaffer, G., Huber, M., Rondanelli, R., & Pepke Pedersen, J. O. (2016). Deep time evidence for climate sensitivity increase with warming. *Geophysical Research Letters*, *43*(12), 6538-6545. doi: https://doi.org/10.1002/2016GL069243

Shell, K. M., Kiehl, J. T., & Shields, C. A. (2008). Using the radiative kernel technique to calculate climate feedbacks in ncar's community atmospheric model. *Journal of Climate*, *21*(10), 2269 - 2282. doi: https://doi.org/10.1175/2007JCLI2044.1

Sherwood, S. C., Webb, M. J., Annan, J. D., Armour, K. C., Forster, P. M., Hargreaves, J. C., … Zelinka, M. D. (2020). An assessment of earth's climate sensitivity using multiple lines of evidence. *Reviews of Geophysics*. doi: https://doi.org/10.1029/

2019RG000678

Smith, C. J., Kramer, R. J., Myhre, G., Alterskjær, K., Collins, W., Sima, A., ... Forster, P. M. (2020). Effective radiative forcing and adjustments in cmip6 models. *Atmospheric Chemistry and Physics*, *20*(16), 9591–9618. doi: https://doi.org/10.5194/acp-20-9591-2020

Soden, B. J., & Held, I. M. (2006). An assessment of climate feedbacks in coupled ocean–atmosphere models. *Journal of Climate*, *19*(14), 3354 - 3360. doi: https://doi.org/10.1175/JCLI3799.1

Soden, B. J., Held, I. M., Colman, R., Shell, K. M., Kiehl, J. T., & Shields, C. A. (2008). Quantifying climate feedbacks using radiative kernels. *Journal of Climate*, *21*(14), 3504 - 3520. doi: https://doi.org/10.1175/2007JCLI2110.1

Tierney, J. E., Zhu, J., King, J., Malevich, S. B., Hakim, G. J., & Poulsen, C. J. (2020, Aug 01). Glacial cooling and climate sensitivity revisited. *Nature*, *584*(7822), 569-573. doi: https://doi.org/10.1038/s41586-020-2617-x

Zhu, J., & Poulsen, C. J. (2021). Last glacial maximum (lgm) climate forcing and ocean dynamical feedback and their implications for estimating climate sensitivity. *Climate of the Past*, *17*(1), 253–267. Retrieved from `https://cp.copernicus.org/articles/17/253/2021/` doi: https://doi.org/10.5194/cp-17-253-2021

Zhu, J., Poulsen, C. J., & Tierney, J. E. (2019). Simulation of eocene extreme warmth and high climate sensitivity through cloud feedbacks. *Science Advances*, *5*(9). doi: https://doi.org/10.1126/sciadv.aax1874

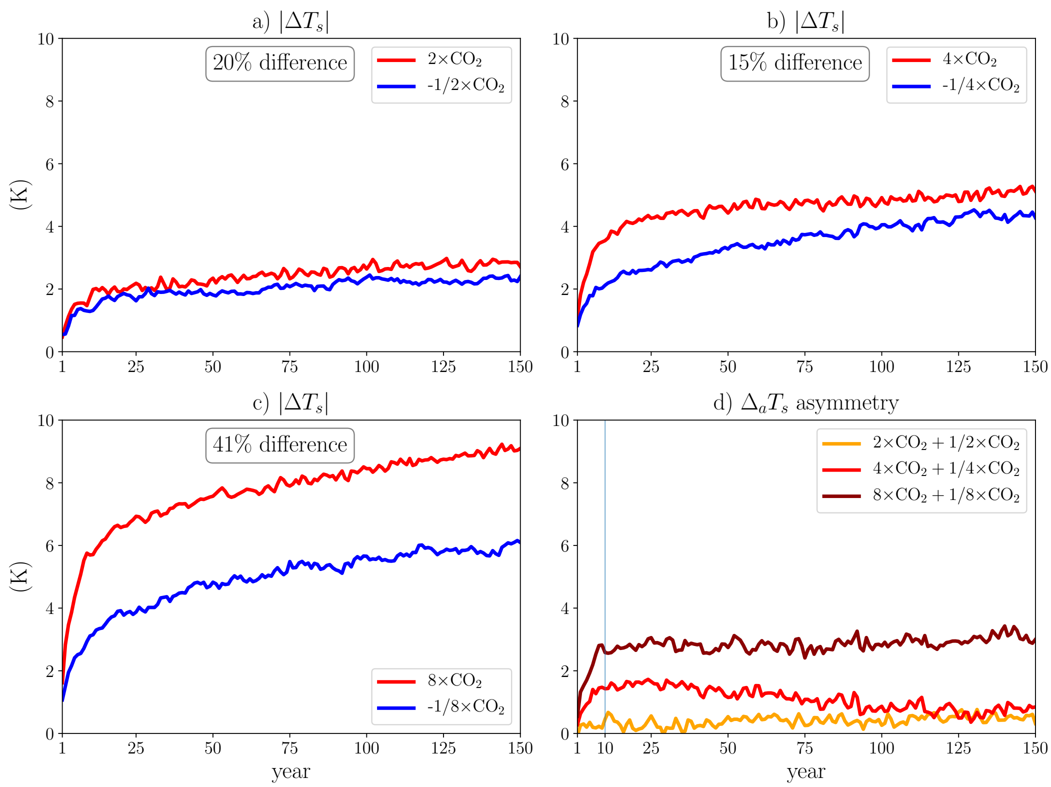

Figure 1. Timeseries of surface temperature response ($|\Delta T_s|$) for abrupt CO_2 runs with CESM-LE model. a) 2×CO_2 and 1/2×CO_2, b) 4×CO_2 and 1/4×CO_2, c) 8×CO_2 and 1/8×CO_2 runs, and d) surface temperature asymmetry ($\Delta_a T_s$) between "warm" and "cold" cases.

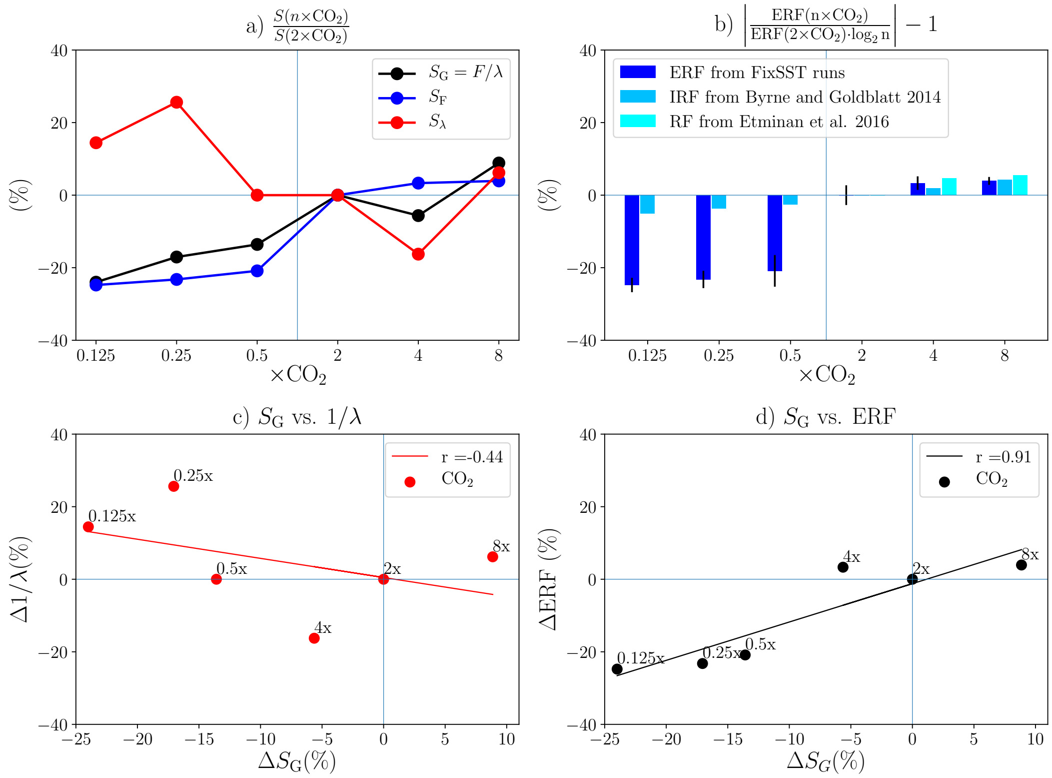

Figure 2. Percent change (from $2\times CO_2$) for abrupt CO_2 runs with CESM-LE model of: a) climate sensitivity as x-intercept of Gregory Regression (black, S_G), as a function of ERF (blue, S_F), and as a function of $1/\lambda$ (red, S_λ); b) effective radiative forcing (dark blue, ERF), instantaneous radiative forcing (IRF) fit from Byrne and Goldblatt (2014) (light blue), and stratospherically adjusted radiative forcing (RF) fit from Etminan et al. (2016) (cyan). c) Percent change of S_G vs. $1/\lambda$ (red) and d) S_G vs. ERF (black). r is the Pearson correlation coefficient.

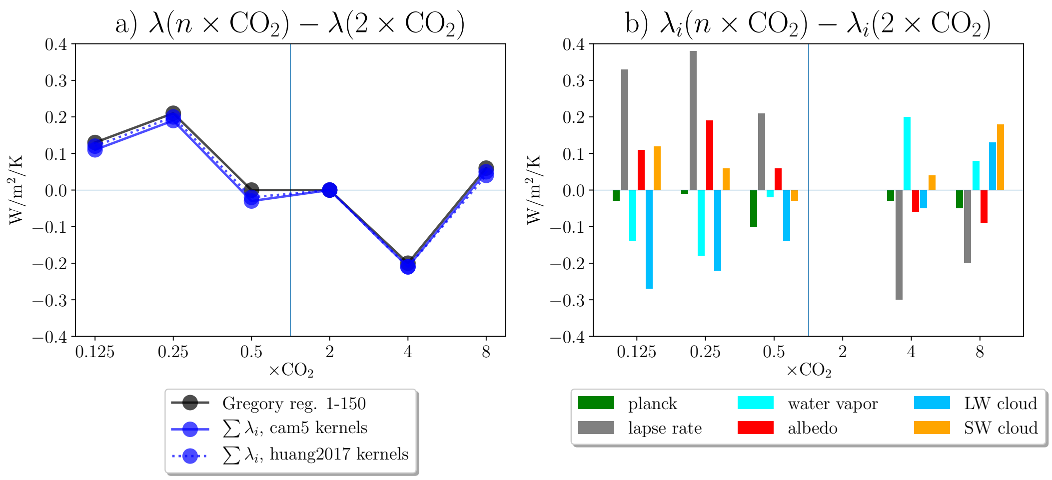

Figure 3. Feedbacks for abrupt CO_2 runs with CESM-LE model are shown as a difference from to $2\times CO_2$. a) Total feedback calculated with Gregory Regression years 1-150 (black), Pendergrass et al. (2018) kernels for CESM1-CAM5 (blue solid), and Huang et al. (2017) kernels (blue dashed). b) Individual feedbacks calculated with Pendergrass et al. (2018) kernels.

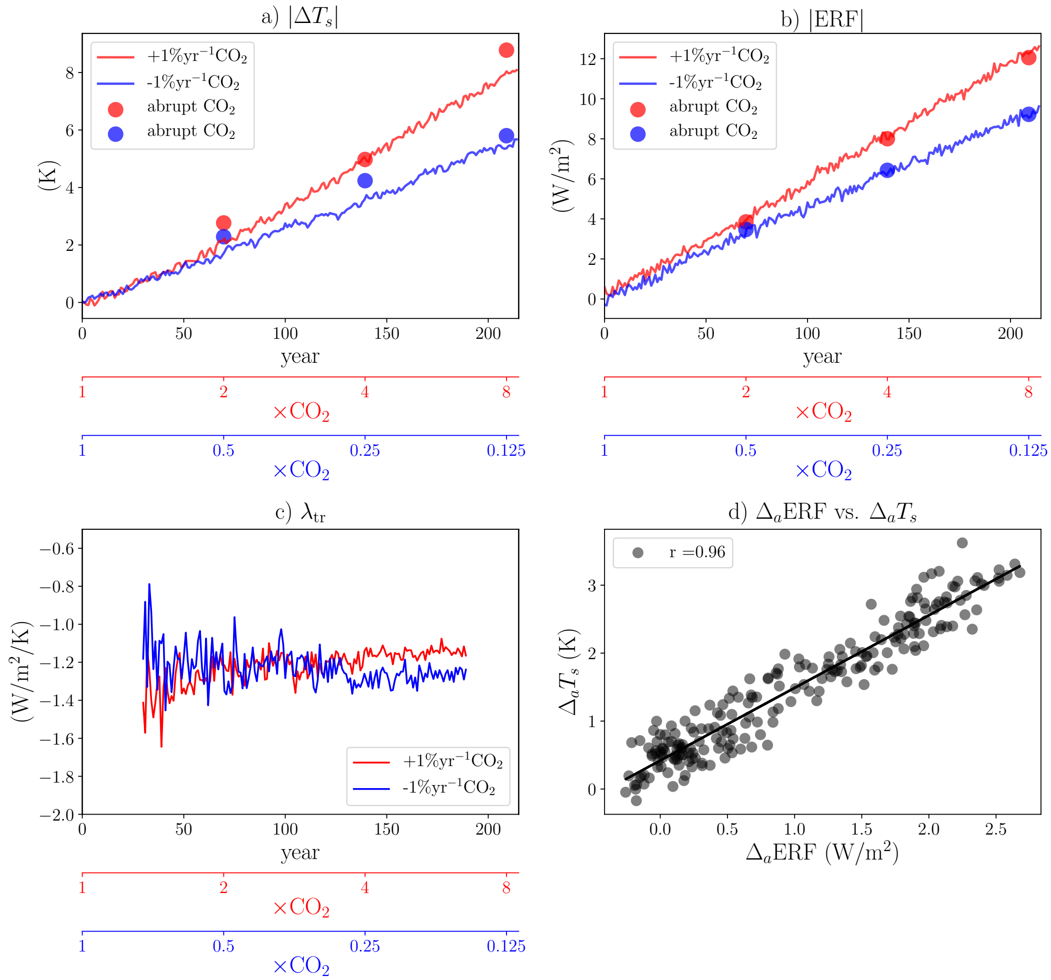

Figure 4. Transient runs annual timeseries with CESM-LE of a) the absolute value of surface temperature response ($|\Delta T_s|$), b) effective radiative forcing (|ERF|), c) net feedback (λ_{tr}), and d) correlation between asymmetries in $\Delta_a T_s$ and Δ_aERF. Responses from abrupt simulations are shown as dots.